ELSEVIER

Contents lists available at ScienceDirect

Materials Chemistry and Physics

journal homepage: www.elsevier.com/locate/matchemphys





Cooperative Pseudo Jahn Teller distortion derives phase transitions in bismuth oxide

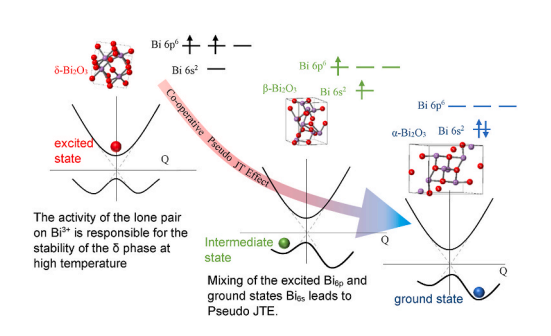
Kelvin Dsouza^a, Daryoosh Vashaee^{a,b,*}

- ^a Electrical and Computer Engineering Department, North Carolina State University, Raleigh, NC, USA
- ^b Materials Science and Engineering Department, North Carolina State University, Raleigh, NC, USA

HIGHLIGHTS

- Bi₂O₃ exhibits four polymorphs of α , β , δ , and γ versus temperature.
- Phase transition in Bi₂O₃ is due to the cooperative pseudo-Jahn Teller effect.
- ELF and COHP data reveal the role of Bi³⁺ lone pair in the 2nd-order phase transition.
- O_{2p} orbital is responsible for stabilizing the lone pair activity.

G R A P H I C A L A B S T R A C T



ABSTRACT

Bismuth oxide exhibits a complex array of structures with a broad range of properties of various technological importance. We derive the phase transition pathway using the in-situ heating X-ray diffraction data, evidencing four polymorphs of α , β , δ , and γ . We prove that the observed phase transitions are due to the cooperative pseudo-Jahn-Teller distortion in the crystal originating from mixing the ground state Bi_{6s} and excited Bi_{6p} states. Using the electron localization function and crystal orbital theory, we explore the role of the Bi_{7}^{3} lone pair in the second-order phase transition. It is found that the O_{2p} states have a critical role in stabilizing the lone pair activity, which leads to a pseudo-Jahn Teller distortion cooperatively inducing the phase transition.

1. Introduction

Bismuth oxide (Bi₂O₃) has been shown to have widely attractive properties such as wide optical bandgap, high refractive index, high dielectric permittivity, and the highest ionic conducting material of all known oxygen ion conductors, making it suitable for applications that range from solid oxide fuel cells [1], gas sensors [2,3], optical coating

[4], catalysis [5,6], and optoelectronics [7]. Bi₂O₃ exists in four polymorphs of α , β , δ , and γ [8,9] with additional structures such as ϵ -Bi₂O₃ (orthorhombic) [10], ω -Bi₂O₃ (triclinic) [11], and η - Bi₂O₃ (hexagonal) [12] reported. The stable room temperature monoclinic α -phase ($P2_1/c$) transforms to the high-temperature face-centered cubic δ -phase ($Fm\overline{3}m$) with a defective CaF₂ structure at 730 °C, which is stable up to the melting point of 850 °C. On cooling, the metastable tetragonal β ($P\overline{4}2_1c$)

^{*} Corresponding author. Electrical and Computer Engineering Department, North Carolina State University, Raleigh, NC, USA. *E-mail address:* dvashae@ncsu.edu (D. Vashaee).

or body-centered cubic γ (i23) can be obtained at 650 °C and 640 °C, respectively, depending on the experimental conditions. The β - α transition occurs at 400 °C, and the γ - α transition occurs at 500 °C [8,13]. Fig. 1 demonstrates this phase transition graphically with respect to temperature. The temperature-dependent XRD shown in Fig. 1 confirms the reported values. †

The 6s² orbitals form the lone pair on the Bi atoms, and the structural transitions and orientations of the stable and metastable phases can be attributed to the positions of these lone pairs. The structural relationship between the different phases of the crystal raises the question of the underlying mechanism governing the phase transitions in this system. The different polymorph phases of bismuth oxide have been stabilized at room temperature by adding various dopant oxides to substitute different sites in the bismuth oxide crystal [14–17]. The stabilization of these phases has been extensively studied, but a fundamental understanding is still lacking.

The Jahn-Teller effect can be defined as the geometrical instability due to the degenerate energy levels of the ion, which ultimately leads to distortion of the crystal field surrounding the ion [18]. In high symmetry systems with non-degenerate energy levels, the distortion can be attributed to the pseudo-Jahn Teller effect [19], which can occur due to the coupling of the ground and excited states. The pseudo-Jahn Teller effect with the possibility of mixing the 2s and 2p orbitals for a single electron in the T state through the τ_{1u} mode was first shown by Opik and Pryce [20]. Orgel showed that a stereochemically active lone pair leads to asymmetric distortion of the octahedra due to the mixing of the s and p states in non-cubic environments lacking a center of symmetry that can affect the chemistry of the related ions [21]. The connection between these distortions and the Jahn-Teller effect for In + ion in the octahedral environment of the InCl crystal was shown by Maaskant [22]. In crystals, these local distortions can affect the system globally, creating a cooperative effect and leading to a phase transition. Phase transitions due to Jahn Teller and pseudo-Jahn Teller effects have been previously reported in the literature [23].

In this work, we investigate the phase transition path followed by the bismuth oxide system by calculating the electron localization function and crystal orbital hamiltonian population to understand the electronic structure. The location and activity of the lone pair are identified computationally. We show how the lone pair system in the higher temperature phase is semi-active due to the hybridization of the Bi–O orbitals and long-range Bi–Bi interaction. Using the results, we demonstrate that the Bi center undergoes a pseudo-Jahn Teller distortion leading to the phase transition path of $\delta{\to}\beta{\to}\alpha$, which is observed in experiments. In this paper, we discuss the transition of $\delta{\to}\beta{\to}\alpha$ as we have shown experimentally through high-temperature XRD and do not discuss the $\delta{\to}\gamma{\to}\alpha$ transition. The stability of the $\gamma{-}$ phase depends mainly on impurities and vacancies in the structure, which have also been discussed by many authors '[8,9,24,25].

2. Computational details

The calculations were carried out using the first principle based on density functional theory (DFT) [26]. We used the generalized gradient approximation (GGA) by Perdew-Burke-Erznerhof (PBE) [27] for the exchange correlation implemented within the projector augmented wave method [28] in the Quantum Espresso package [29,30]. A plane

wave cutoff of 500 eV was implemented with k-point grid density using the Monkhorst Pack [31] method of $5\times5\times5$ used for $\alpha\text{-Bi}_2O_3$ and $6\times6\times6$ for $\beta\text{-Bi}_2O_3$ and $\delta\text{-Bi}_2O_3$ configurations. The structural optimization was carried out by fitting the energy volume curve to the Murnaghan equation of state [32]. The position of the atoms was optimized such that the forces between each atom converged to 0.0006 eV. The density of states, electron localization function, and band structure for the electrons were computed using the post-processing tool in Quantum Espresso.

The electron localization function, as shown by Becke and Edge-combe[33], is the measure of the probability of finding an electron in the vicinity of another electron. This can provide information about the core, bonding, non-bonding, and lone pairs in the real space for different regions in the crystal. The electron localization function (ELF) for the Kohn-Sham orbitals ψ_i and electron density ρ is given by Silvi and Savin [34], defined as:

$$ELF = \frac{1}{1 + \left(\frac{D}{D_h}\right)^2}$$

whore

$$D = \frac{1}{2} \sum_{i} |\nabla \psi_{i}|^{2} - \frac{1}{8} \frac{|\nabla \rho|^{2}}{\rho}$$

$$D_h = \frac{3}{10} (3\pi^2)^{5/3} \rho^{5/3}$$

ELF is a dimensionless quantity that varies from 0 to 1 and is close to 1 for regions occupied by paired electrons. ELF has been used to visualize bonding in solids and to study lone pair distortion in different crystal systems [35,36].

To visualize the local chemical bonding in energy-resolved regions using density functional theory, Crystal Orbital Hamiltonian Population (COHP) [37] has found many exciting applications. COHP analysis gives information regarding bonding, antibonding, and non-bonding energy regions, along with the contribution of an atom to the distribution of energies. On the interpretation of the COHP data, a positive COHP value indicates bonding in the energy region, and a negative COHP corresponds to antibonding. The computer program LOBSTER [38–40] is used for calculating the COHP in different configurations.

The distortion around the lone pair is caused by the interaction between the s and p orbitals of the anion and is mediated by the p orbitals of the cation. This can also be interpreted as a double pseudo-Jahn Teller effect [41]. The pseudo-Jahn-Teller effect can be evaluated by calculating the effective force constant, as shown by Bersuker and Polinger [15,42]

$$K = \langle \psi_0 \left| \frac{\partial^2 H}{\partial Q^2} \right| \psi_0 \rangle - 2 \sum_n \frac{\left| \langle \psi_0 \left| \frac{\partial H}{\partial Q} \right| \psi_n \rangle \right|^2}{E_n - E_o}$$

Where H is the Hamiltonian, Q is the normal coordinate, ψ_0 is the non-degenerate ground state, and ψ_n is the excited state. The first term corresponds to the APES, considering the Born-Oppenheimer approximation. The second term contributes to the instability of the system, which is the off-diagonal vibronic coupling constant.

3. Results

The relaxed structure of different phases of ${\rm Bi}_2{\rm O}_3$ is shown in Table 1. The calculated lattice parameters were within tolerance with the experimentally determined values.

4. δ- Bi₂O₃

The δ phase of bismuth oxide is the best-known ion conductor, but

 $^{^\}dagger$ The sample of $\rm Bi_2O_3$ was procured from Sigma Aldrich (99.99%). The temperature dependent XRD was conducted using PANalytical Empyrean Diffractometer using a standard Bragg-Brentano geometry, 40 kV acceleration voltage, 44 mA current, and a step size of 0.02°with provision for high-temperature measurement. The data was collected at the heating rate of 10 deg/min from 25 °C to 600 °C and 5 deg/min from 600 °C to 750 °C. The cooling rate was set at 5 deg/min from 750 °C to 500 °C and 10 deg/min from 500 °C to 25 °C.

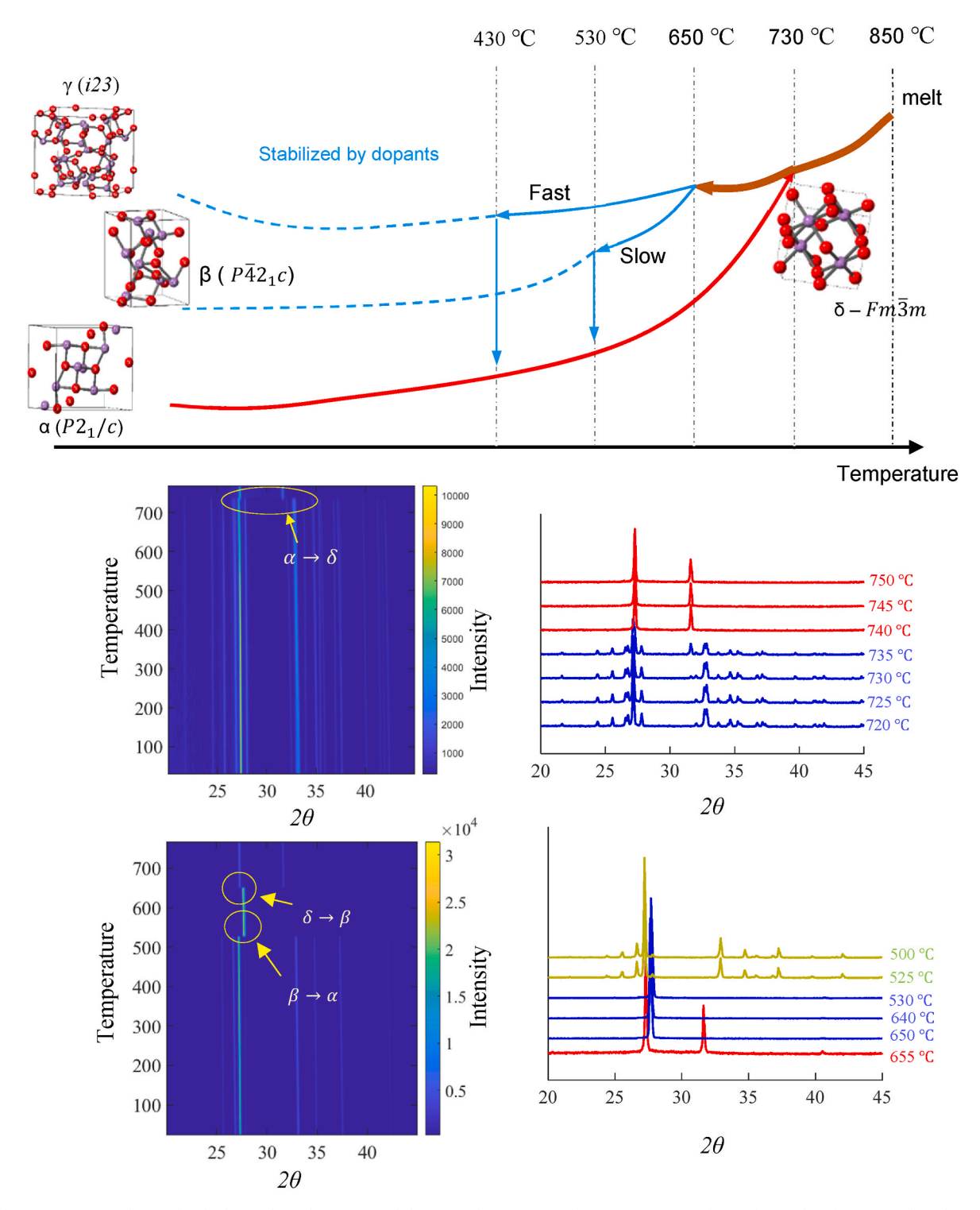


Fig. 1. Phase transition pathways for the bismuth oxide system and the in-situ heating XRD data. Bi_2O_3 exists in four polymorphs of α , β , δ , and γ . The stable room temperature monoclinic α -phase $(P2_1/c)$ transforms to the high-temperature face-centered cubic δ -phase $(Fm\overline{3}m)$ with a defective CaF₂ structure at 730 °C, which is stable up to the melting point of 850 °C. On cooling, the metastable tetragonal β ($P\overline{4}2_1c$) or body-centered cubic γ (i23) can be obtained at 650 °C and 640 °C, respectively, depending on the experimental conditions. The β - α transition occurs at 400 °C, and the γ - α transition occurs at 500 °C.

due to its instability at room temperature, it places a limitation on the application in solid oxide fuel cells. It is usually doped with lanthanide oxides to stabilize it at lower temperatures, but that decreases its ionic conductivity [48]. The δ phase adopts a defective CaF₂ structure, where the high ionic conductivity is attributed to the ordered oxygen vacancies in the system. The oxygen vacancies in the δ structure are ordered in three possible alignments <100>, <110>, and <111> [39,41]

The oxygen vacancy sites for each vacancy arrangement in the $\delta\text{-Bi}_2\mathrm{O}_3$ crystal lattice are shown in Fig. 2(a–c). The ELF plot in the Bi–Bi plane is given in Fig. 2(d–f), and the O–O plane is given in Fig. 2(g–i). The deep blue color in the ELF plot signifies the extreme where the localization probability is minimum, and the red color signifies the maximum probability. The PAW calculation considers only the valence electrons with [He]2s^22p^2 and [Xe]5d^{10}6s^2 for the O and Bi atoms,

Table 1Calculated and experimental structural properties for different phases of bismuth oxide [9,13,43–47].

		Space group	Lattice Parameters Å Calculated (Expt)		Volume (Å ³)
α- Bi ₂ O ₃		$P2_1/c$	a = 5.9498 (5.8458)	$\alpha = \gamma = 90 \ (90)$	346.101
			b = 8.3275 (8.1656)	$\beta = 112.473 \ (112.969)$	
			c = 7.5594 (7.5077)		
β- Bi ₂ O ₃		$P\overline{4}2_1c$	a = 7.8791 (7.7439)	$\alpha = \beta = \gamma = 90 \ (90)$	357.182
			b = 7.8791 (7.7439)		
			c = 5.7536 (5.6287)		
δ- Bi ₂ O ₃	<100>	Fm3m	a = 5.3760 (5.6607)	$\alpha=\beta=\gamma=90~(90)$	161.180
			b = 5.3760 (5.6607)		
			c = 5.5768 (5.6607)		
	<110>	Fm3m	a = 5.8653 (5.6607)	$\alpha=\beta=\gamma=90~(90)$	165.627
			b = 5.5342 (5.6607)		
			c = 5.5342 (5.6607)		
	<111>	$Fm\overline{3}m$	a = 5.4589 (5.6607)	$\alpha=\beta=\gamma=90~(90)$	162.672
			b = 5.4589 (5.6607)		
			c = 5.4589 (5.6607)		

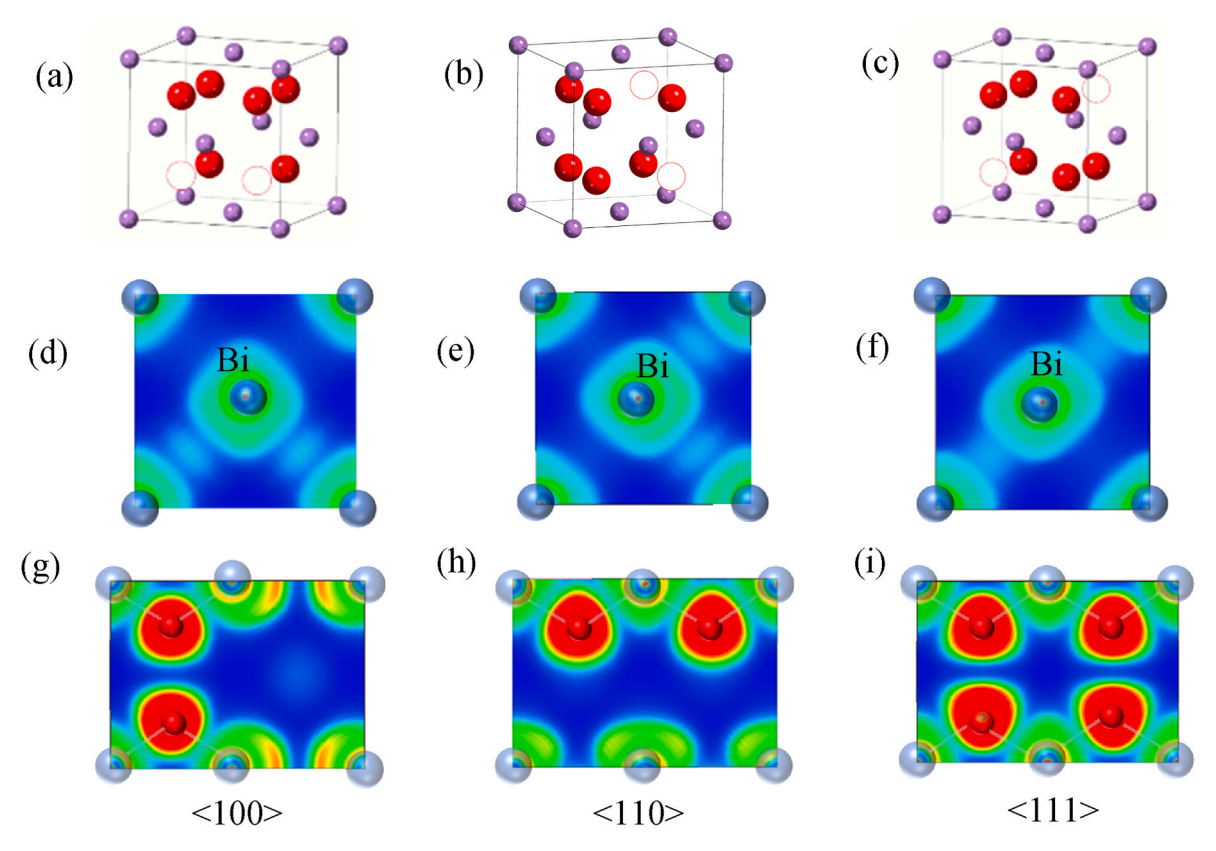


Fig. 2. δ -Bi₂O₃: (a–c) The crystal structures indicating the different vacancy configurations (empty red circles). (d–f) The ELFs projected on the Bi–Bi plane are shown. The asymmetry is seen in the <100> and <110> configurations, whereas the <111> direction is perfectly symmetric across the diagonal. (g–i) The ELFs projected on the O–O plane are shown with bonding between the Bi–O atoms. (For interpretation of the references to color in this figure legend, the reader is referred to the Web version of this article.)

respectively. The deep red on the O atom in the O–O plane can be attributed to the $2s\ ^22p^2$ state.

The ELF plot gives us information regarding the type of bonding between the Bi–O atom. Based on the ELF plot in the O–O plane, we can see a lone pair attractor basin between the Bi–O atom indicating a single σ bond between these atoms. The σ bond can result from the s-p hybrid bond between Bi $_{6s}$ – O_{2p} and a p-p bond between Bi $_{6p}$ – O_{2p} . The high symmetry of the structure can point towards the Bi $_{6p}$ – O_{2p} being present in the system. The ELF in the Bi–Bi plane around the <100> and <110> configuration shows a slight asymmetric distribution with its lobe pointing towards the Bi atom at the vertices of the lattice. The <111> configuration has a symmetric configuration stretched along the

diagonals. Based on the ELF plots, we can confirm a long-range Bi–Bi interaction exists. The electron density across the O–O plane for the $\delta\text{-Bi}_2O_3$ configurations, which is given by Walsh et al. [49], demonstrated an asymmetric electron density in the <100> and <110> configuration and symmetric in the <111> configuration, attributed to active and inactive lone pairs, respectively. In this result, we show that the lone pair is absent in $\delta\text{-Bi}_2O_3$, and the long-range Bi–Bi interactions result in asymmetry in the <100> and <110> phases.

We calculate the COHP and partial density of states for the Bi and O orbitals to investigate the bonding between the Bi–O and to investigate the availability of energy states. The COHP plot for the different δ configurations is presented in Fig. 3, showing the level of mixing

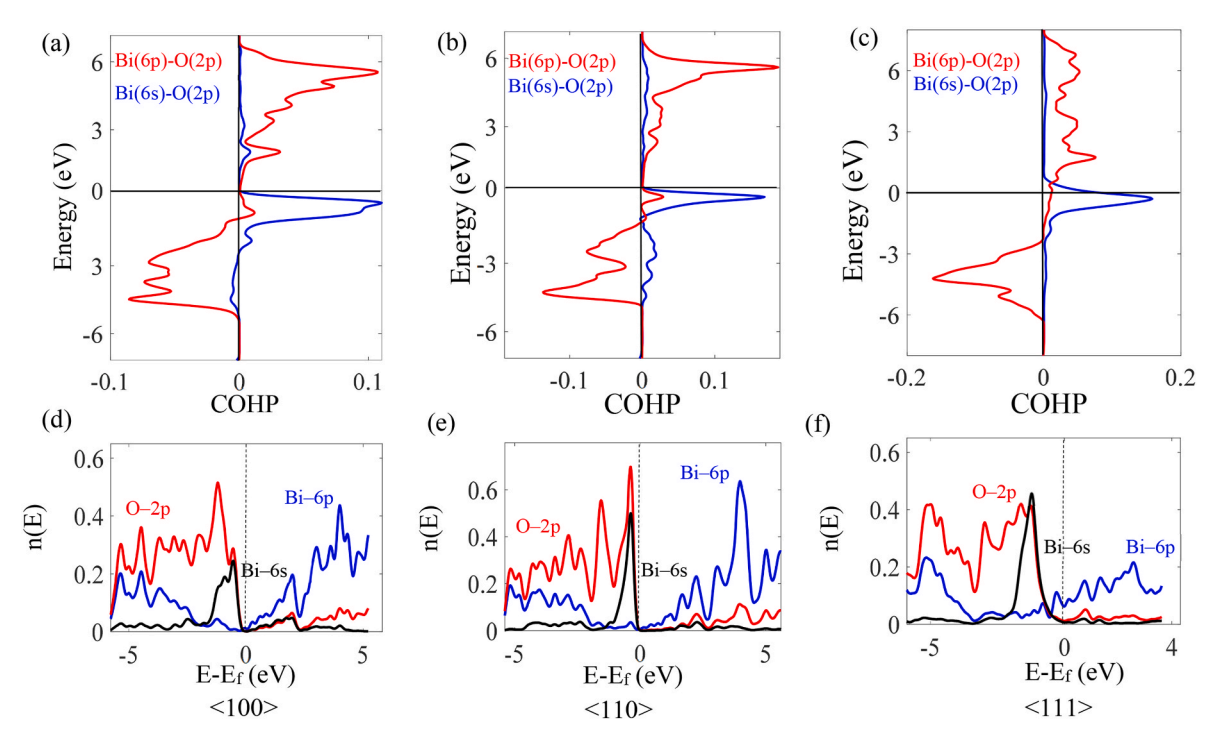


Fig. 3. δ -Bi₂O₃: Crystal Orbital Hamiltonian Populations for <100>, <110>, and <111> are given in (a–c) respectively for Bi_{6p}-O_{2p} (red) and Bi_{6s}-O_{2p} (blue). The partial density of states for <100>, <110> and <111> are given in (d–f) respectively Bi_{6p} (blue), O_{2p} (red), Bi_{6s}(black). (For interpretation of the references to color in this figure legend, the reader is referred to the Web version of this article.)

between the different energy states. For the $<\!100>$ and $<\!110>$ configurations, there is a strong bonding between the Bi $_{6s}$ - O_{2p} states, with a peak also seen for the bonding between Bi $_{6p}$ - O_{2p} orbitals near the valence bands. In the conduction band, we have strong bonding characters for Bi $_{6p}$ - O_{2p} orbitals, with the bonding between Bi $_{6s}$ - O_{2p} significantly reduced. The partial density of states $<\!100>$ and $<\!110>$ show peaks for the Bi $_{6s}$ and O_{2p} near the top of the valence band with reduced contribution from the Bi $_{6p}$ states. The available Bi $_{6p}$ states significantly increase in the conduction band compared to the Bi $_{6s}$ states. The COHP for the $<\!111>$ configuration indicates a bonding between the two orbitals at the valence band and into the conduction band. The partial density of states for the $<\!111>$ configuration shows a flat band across the Fermi level for the Bi $_{6p}$, with the states significantly increasing in the conduction band. This can be seen as a semi-metallic behavior for the $<\!111>$ configuration.

In the δ configuration, the ELF plot shows evidence of an inactive lone pair, and the COHP plot shows a bonding state $Bi_{6s}/Bi_{6p}-O_{2p}$ in the conduction band close to the Fermi energy. As the phase is stable at high temperatures, the high energy mixing between the Bi_{6s} and Bi_{6p} can be concluded. Medvedeva et al. also showed that the Bi–O hybridizes

through the $Bi_{p_xp_yp_z}$ with the neighboring oxygen atoms through the Bi_{6p} - O_{2p} orbital, which confirms our result [38].

5. β -Bi₂O₃

 β -Bi₂O₃has a wide bandgap and shows excellent photocatalytic activity under visible light [50,51]. The crystal lattice of the β -Bi₂O₃ can be considered as an ordered superstructure of the cubic fluorite arrangement with the oxygen vacancies ordered in the <111> and <100> direction [42,52]. The Bi–O₄ trigonal pyramids are linked via oxygen atoms to give empty channels at (0,0, z) and (1/2,1/2, z). The lone pairs are directed toward these channels. β - Bi₂O₃ has a direct bandgap and was calculated to be 1.8 eV compared to the experimental value of 2.58 eV [53].

The ELF plot for the β phase is shown in Fig. 4 along the Bi–Bi plane. The asymmetric distribution in ELF indicates where the lone pair is located at the (½½ z) channel; Laarif and Theobald have calculated the position of the lone pair by using the geometric examination of the bond distances at the same location [54]. The lone pairs are oriented toward each other, which is not usually expected as the coulomb repulsion due

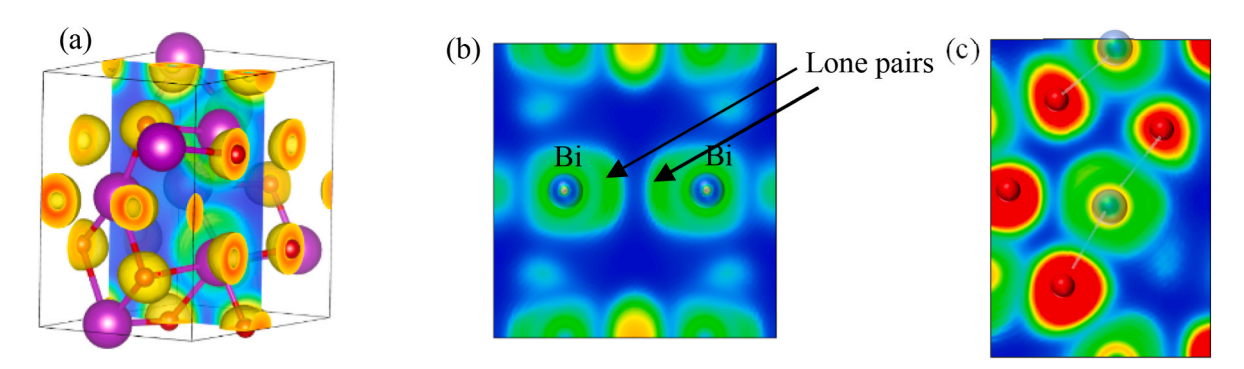


Fig. 4. β-Bi₂O₃: (a) The ELF in 3D along the Bi–Bi plane, (b) 2D display of the ELF plot across the Bi–Bi plane, and (c) 2D display of the ELF plot across the O–O plane. The asymmetric distribution of the ELF indicates the position of the lone pair at each view, as pointed by arrows.

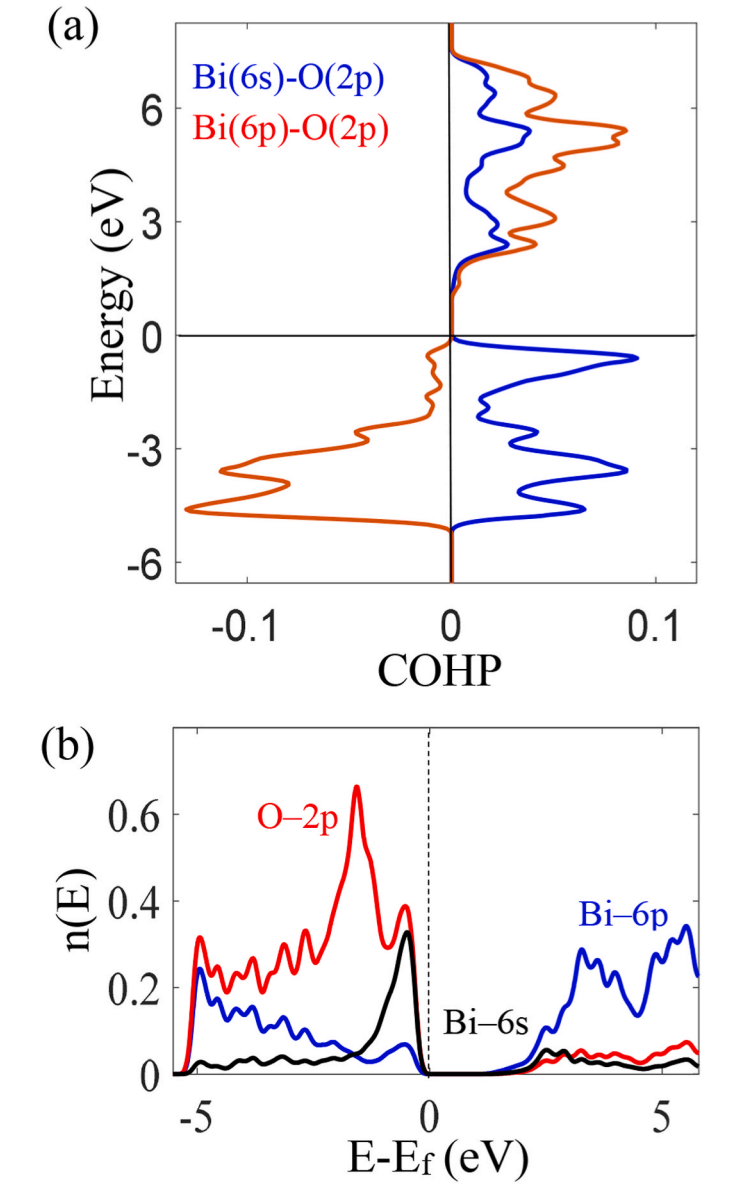


Fig. 5. β-**Bi**₂O₃: (a) Crystal Orbital Hamiltonian Population (COHP) for with the bonding character of Bi_{6p} -O_{2p} (red) and Bi_{6s} -O_{2p} (blue). (b) The partial density of states for the orbitals Bi_{6p} (blue), O_{2p} (red), Bi_{6s} (black). (For interpretation of the references to color in this figure legend, the reader is referred to the Web version of this article.)

to the lone pair electron charge should orient them away from each other. The ELF in the O–O plane is shown in Fig. 4, displaying the σ bonding between the Bi–O atoms. The Bi–O hybridization of the sp orbital can follow as an increased spread in the distribution of the electrons resulting in a semi-active lone pair.

The COHP plot in Fig. 5 demonstrates a Bi_{6s} - O_{2p} bonding state and Bi_{6p} - O_{2p} antibonding state below the Fermi level. The conduction band show bonding for both states. In this system, the high energy state is the bonding/antibonding state between Bi_{6p} - O_{2p} orbitals, and the ground state is the bonding between Bi_{6s} - O_{2p} orbitals. The partial density of states shows peaks in the O_{2p} , Bi_{6s} , and Bi_{6p} in the valence band, with increased states of Bi_{6p} in the conduction band. The β - $Bi_{2}O_{3}$ is a high-temperature phase stable at $630^{\circ}C$ - $450^{\circ}C$, which can lead to the hybridization of the Bi_{6s} and Bi_{6p} with the O_{2p} atoms. As the Pseudo Jahn Teller is due to the mixing of the ground and excited states, we can assume the excited states to be the bonding between the Bi_{6p} - O_{2p} atoms.

6. α -Bi₂O₃

The monoclinic α -phase is the ground state phase for Bi₂O₃. The α -Bi₂O₃ is a subject of significant research, and one may find a great deal of literature [2,3,55]. The lone pair activity around the Bi atom greatly influences a highly irregular structure found in this phase. The α -phase has an indirect bandgap with a calculated value of 2.05 eV compared to the experimental value of 2.85 eV [56].

The ELF plot across the Bi–Bi plane shown in Fig. 6 has an asymmetric distribution indicating an active lone pair. Contrary to the $\beta\text{-Bi}_2O_3$ the lone pair is oriented away from the Bi atoms. The O–O plane show bonding between the Bi and O atoms, but a reduction in the lone pair attractor basin can be seen. The volume of the $\alpha\text{-phase}$ is larger than its higher temperature phases. The COHP plot shows a Bi_{6s}-O_{2p} bonding and Bi_{6p}-O_{2p} antibonding at the valence bands, similar to the β phase and bonding in the conduction band. The partial density of states shows the overlapping O_{2p} and Bi_{6s} near the Fermi level, with the excited states still dominated by the Bi_{6p} states. Contrary to the β phase, there are additional peaks in the Bi_{6p}, Bi_{6s}, and O_{2p} close to the Fermi level (see Fig. 7).

7. Discussion

Analysis of vibronic interaction can help study the structural deformation resulting from the phase transition. The distortion in the local Bi-O bonds is determined by the activation of the lone pair electrons and the direction it traverses to achieve stability. The PJT problem is the 2level problem for the ground and excited state. The strong vibronic coupling between the ground and excited states leads to the ground state instability. The local destabilizing force due to the mixing of the ground and excited states induced by the pseudo-Jahn Teller effects results in a cooperative effect in the crystal, ultimately leading to the phase transition. By studying the cooperative pseudo-Jahn Teller effect, we can accurately describe the distortion modes and reveal different structures that can be accessible to the system but not thermodynamically favored. By employing the argument of cooperative pseudo-jahn teller effect, the stabilization of the high temperature phases of Bi₂O₃ by different dopants can be explained as an inherent cancellation of the pseudo-jahn teller distortion due to the reduction in the cooperative effect in the cooperative effect.

8. δ - β Transformation

The ELF and COHP calculation showed that the high symmetry δ -phase has a mixture of Bi_{6s}- O_{2p} and Bi_{6p}- O_{2p} states. The deformation on the local Bi- O_6 octahedra in the δ -Bi₂ O_3 phase can be represented by the local symmetry with point group O_h . The energy diagram in Fig. 8 shows that the δ -phase belongs to the O_h point group with the LUMO in the T_{Iu} mode and the HOMO in the A_{Ig} mode.

In the case of Bi–O₆, the ground state A_{1g} (HOMO) holds the $6s^2$ lone pair couples with the T_{1u} excited state. As the excited state is degenerate, it leads to a JT effect within itself, and the problem can be a combination of the PJ + JT effect. This problem was shown by Bersuker [57] as (A + T) \otimes (a_{1g} + e_g + t_{2g} + t_{1u}). As the e_g and t_{2g} do not couple to the A_{1g} and T_{1u} terms, we can consider a pure PJT problem to get an $(A_{1g} + T_{1u}) \otimes t_{1u}$ problem.

The T_{1u} has three functions given by $|x\rangle$, $|y\rangle$, and $|z\rangle$, and the A_{1g} can be given by $|s\rangle$ as shown in Fig. 9(a-b), leading to three components of the displacements as Q_x , Q_y , and Q_z . The vibronic force constant can be calculated as

$$F = \langle A_{1g} \left| \frac{\partial H}{\partial O_i} \right| T_{1u} \rangle i = x, y, z$$

Following Bersuker [55], the APES in the dimensional t_{1u} space is solved with a two-dimensional trough of equipotential minima points, as

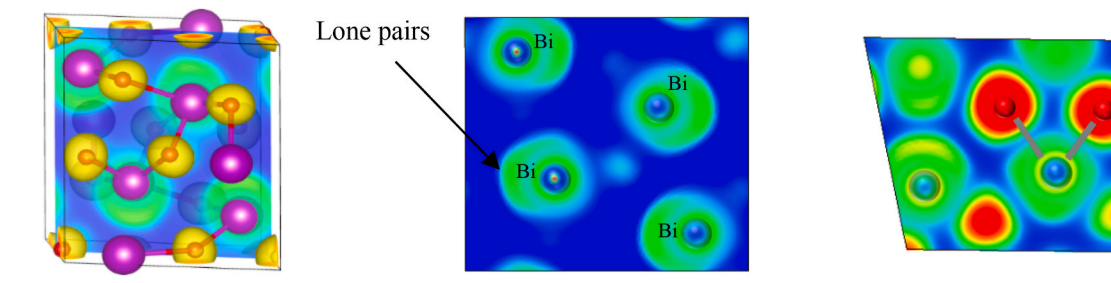


Fig. 6. α-Bi₂O₃: (a) The ELF in 3D along the Bi–Bi plane, (b) 2D display of the ELF plot across the Bi–Bi plane, and (c) 2D display of the ELF plot across the O–O plane.

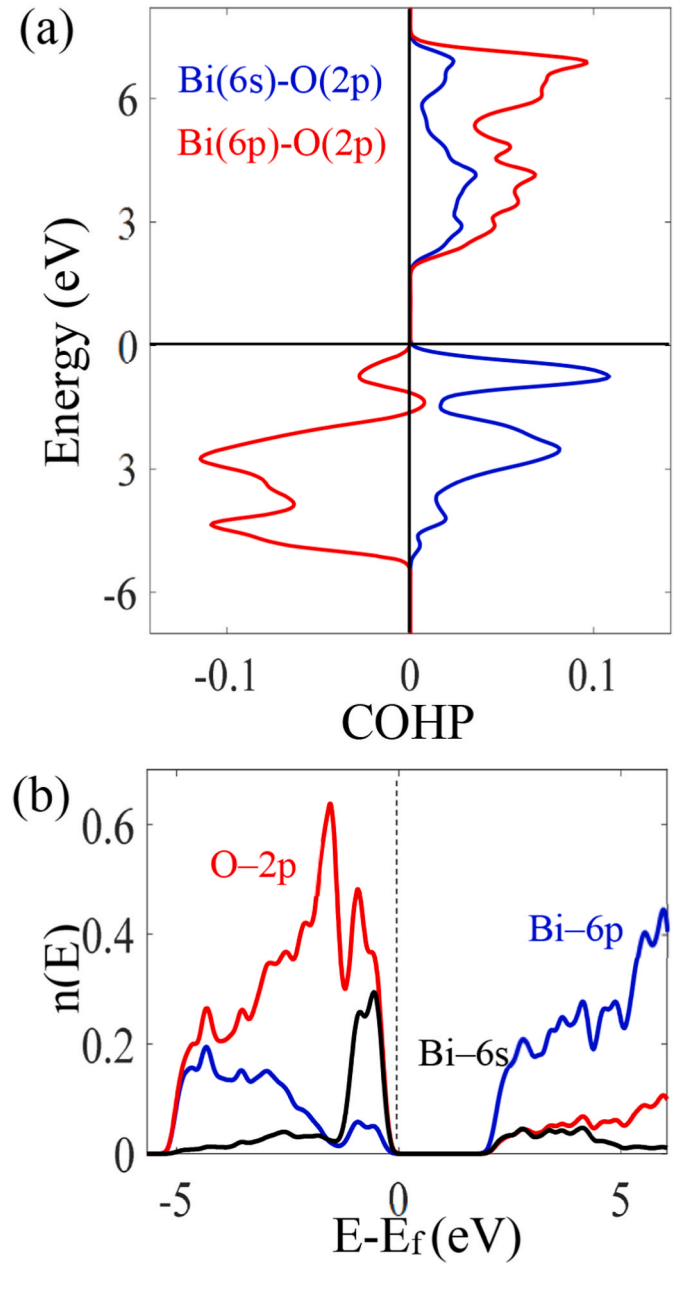


Fig. 7. α-**Bi**₂O₃: (a) Crystal Orbital Hamiltonian Population (COHP) with the bonding character of Bi_{6p}-O_{2p} (red) and Bi_{6s}-O_{2p} (blue). (b) The partial density of states for the orbitals Bi_{6p} (blue), O_{2p} (red), Bi_{6s} (black). (For interpretation of the references to color in this figure legend, the reader is referred to the Web version of this article.)

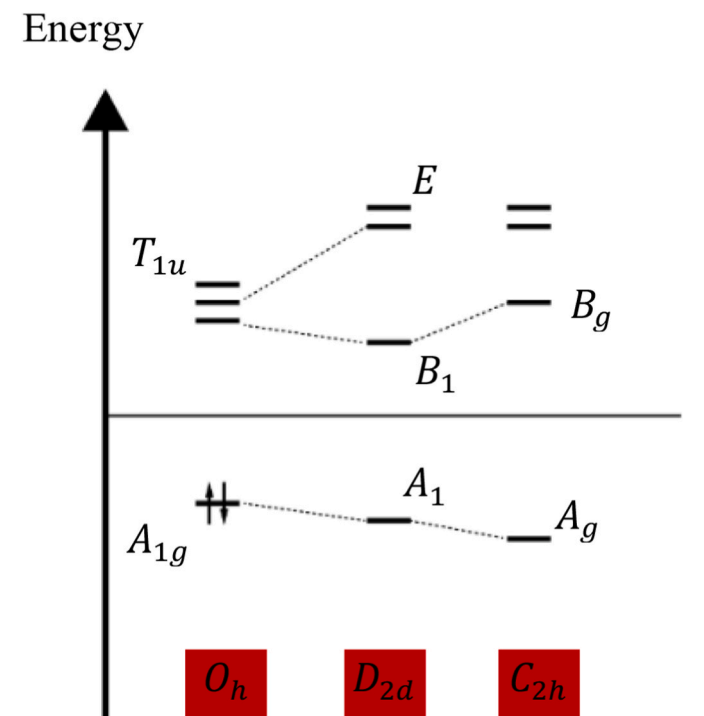


Fig. 8. Energy diagram for different phases of bismuth oxide based on the point groups. The cubic δ-phase is given by the O_h point group, the β-phase is given by the D_{2d} point group, and the monoclinic α-phase is given by the C_{2h} point group.

shown in Fig. 9(c). The minima indicate a tetragonal distortion based on the crystal structure of the β -phase.

The stabilization of the δ phase can be achieved by doping with a system to break the cooperative effect for the corresponding distortion.

9. β-α Transformation

Next, we explore the effect of the lone pair on the β to α transition. The lone pair around the Bi is asymmetric in the β -phase but was shown to have a wider distribution than the α -phase indicating a semi-active lone pair. The ELF plot also showed the direction of the lone pair to point towards the neighboring Bi atom lone pair, and long-range Bi–Bi interaction can be seen to be present, which is mediated through the Bi_{6s}-O_{2p} hybridization. Based on the energy diagram in Fig. 8, the β -phase belongs to the D_{2d} point group with the LUMO in the B_{1} mode, and the HOMO with the lone pair is in the A_{1} mode. The direction of distortion in a lone pair active system is usually in the direction of the lone pair as it offers a path of the lowest energy for diffusion. Fig. 10(a) shows the lone pair location based on the ELF plot. The ground state

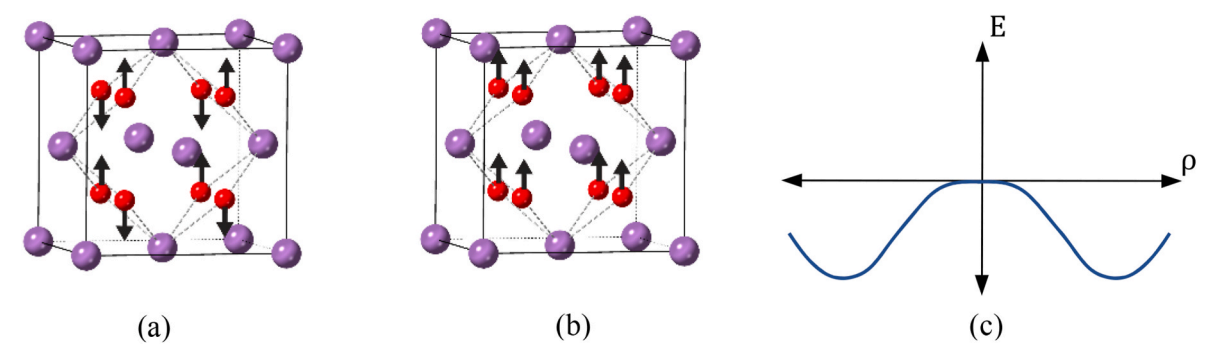


Fig. 9. Vibration modes of δ-Bi₂O₃: (a) A_{1g} and (b) T_{1u} modes in the z-direction are shown. The direction of motion for the oxygen atoms in the vibration modes for ground and excited states are calculated using character projected operators using group theory [58]. (c) The APES for the $A_{1g} + T_{1u}$.

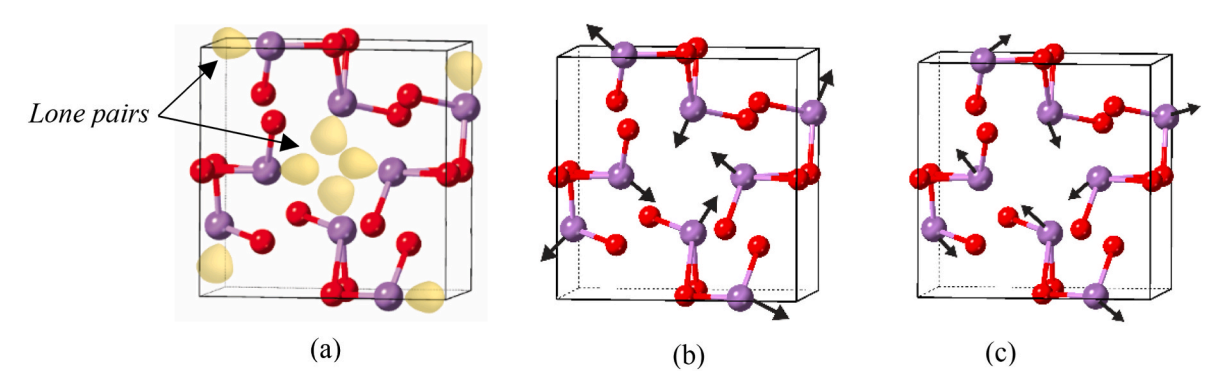


Fig. 10. (a) Lone pair locations are shown as yellow lobes based on ELF calculation. (b) A_1 and (c) B_1 vibrational modes for the Bi atom (purple) show the direction preferred in the β-Bi₂O₃ crystal structure. (For interpretation of the references to color in this figure legend, the reader is referred to the Web version of this article.)

vibration of A_1 is seen to orient towards the lone pair space. The Pseudo Jahn-Teller problem is given by $(A_1+B_1)\otimes b_I$ where the ground and excited state couple through the b_I mode.

A similar treatment of calculating the vibronic constant can be conducted for the β -phase. A more straightforward analysis can be done based on the treatment of strain in the crystal and how it couples with the elastic modes. The quadratic representation of the A_1 mode is $|x^2+y^2\rangle$, and the B_1 mode is given as $|x^2-y^2\rangle$, which can be classified as a symmetry-adapted strain. The $|x^2+y^2\rangle$ can be defined as the symmetry retaining strain and the $|x^2-y^2\rangle$ can be classified as the symmetry-breaking strain. The mixing of these two strains can be attributed to the PJTE. The b_1 mode couples these two strains with the elastic mode, leading to a symmetry breaking in the crystal and, consequently, the structural phase transition.

10. Conclusion

The phase transition pathway chosen by bismuth oxide was investigated experimentally and theoretically. It was found that the phase transition relies primarily on the lone pair system. We demonstrate how the lone pair system evidences the existence of the pseudo-Jahn Teller effect, leading to phase transition in the crystal. Through the ELF calculations, we predict the location of these lone pairs, and through COHP calculations, we confirm the bonding and antibonding between the orbitals. Investigating the electronic structure of different phases of bismuth oxide, we find that the coupling between the ground state Bi-6s and excited states Bi-6p creates instability leading to a pseudo-Jahn Teller distortion and the phases observed experimentally. The transition from the cubic δ -phase to the tetragonal β -phase is posed as a pseudo-Jahn-teller problem given as $(A_{1g}+T_{1u})\otimes t_{1u}$, which shows the coupling through the A_{1g} and T_{1u} state through the t_{1u} mode. Similarly, the $\beta{\to}\alpha$ transition is posed as $(A_1+B_1)\otimes b_1$ problem with coupling the

A₁ and B₁ state through the b₁ mode.

CRediT authorship contribution statement

Kelvin Dsouza: Conceptualization, Methodology, Software, Visualization, Data curation, Writing – original draft, Investigation. **Daryoosh Vashaee:** Writing – review & editing, Investigation, Supervision, Validation, Resources, Funding, Project administration.

Declaration of competing interest

The authors declare the following financial interests/personal relationships which may be considered as potential competing interests: Daryoosh Vashaee reports financial support was provided by Air Force Office of Scientific Research. Daryoosh Vashaee reports financial support was provided by National Science Foundation.

Data availability

Data will be made available on request.

Acknowledgement

This study is partially based upon work supported by the Air Force Office of Scientific Research (AFOSR) under contract number FA9550-19-1-0363 and the National Science Foundation (NSF) under grant numbers CBET-2110603.

References

- A.M. Azad, S. Larose, S.A. Akbar, Bismuth oxide-based solid electrolytes for fuel cells, J. Mater. Sci. (1994) 29 4135–4151.
- [2] A. Cabot, A. Marsal, J. Arbiol, J.R. Morante, Bi2O3 as a selective sensing material for NO detection, Sens. Actuators, B 99 (2004) 74–89.

- [3] Z.N. Adamian, H. v Abovian, V.M. Aroutiounian, Smoke sensor on the base of Bi₂O₃ sesquioxide, Sensor. Actuator. B 35 (1996).
- [4] T. Takeyama, N. Takahashi, T. Nakamura, S. Ito, Growth of the high reflectivity Bi₂O₃ glass films by atmospheric pressure halide CVD, in: Optical Materials, vol. 26, Elsevier, 2004, pp. 413–415.
- [5] T.A. Hanna, The role of bismuth in the SOHIO process, Coord. Chem. Rev. 248 (2004) 429–440.
- [6] N. Arora, G. Deo, I.E. Wachs, A.M. Hirt, Surface aspects of bismuth-metal oxide catalysts, JOURNALS OF CATALYSIS 3 (1996).
- [7] C.L. Gomez, et al., Opto-electronic properties of bismuth oxide films presenting different crystallographic phases, Thin Solid Films 578 (2015) 103–112.
- [8] E.M. Levin, R.S. Roth, Polymorphism of bismuth sesquioxide. I. Pure Bi₂O₃, J Res Natl Bur Stand A Phys Chem 68A (2) (1964 Mar-Apr) 189–195.
- [9] H.A. Harwig, On the structure of bismuthsesquioxide: the α , β , γ , and δ -phase, Z. Anorg. Allg. Chem. 444 (1978) 151–166.
- [10] N. Cornei, N. Tancret, F. Abraham, O. Mentré, New ε-Bi2O3 metastable polymorph, Inorg. Chem. 45 (2006) 4886–4888.
- [11] A.F. Gualtieri, S. Immovilli, M. Prudenziati, Powder X-ray diffraction data for the new polymorphic compound ω- Bi₂O₃, Powder Diffr. 12 (1997) 90–92.
- [12] T. Locherer, et al., High-pressure structural evolution of HP-Bi₂O₃, Phys. Rev. B Condens. Matter 83 (2011).
- [13] F. Schröder, N. Bagdassarov, F. Ritter, L. Bayarjargal, Temperature dependence of Bi_2O_3 structural parameters close to the α - δ phase transition, Phase Transitions 83 (2010) 311–325.
- [14] Turkoglu Orhan, Mustafa Soylak, Synthesis of β and δ phases of Bi₂O₃ stabilized by Gd₂O₃, Asian J. Chem. 14 (2002) 3–4.
- [15] Naixiong Jiang, Eric D. Wachsman, Eric D. Wachsman, Structural stability and conductivity of Phase-stabilized cubic bismuth oxides, J. Am. Ceram. Soc. 82 (11) (1999) 3057–3064.
- [16] M.J. Verkerk, K. Keizer, A.J. Burggraaf, High oxide ion conduction in sintered oxides of the system Bi₂O₃-Er2O3" J, Electrochem. Soc. 10 (1980) 81–90.
- [17] T. Takahashi, H. Iwahara, Y. Nagai, High oxide ion conduction in sintered Biz03 containing SrO, CaO, and La₂O₃, J. Appl. Electrochem. 2 (1972) 97–104.
- [18] I. Bersuker, The Jahn-Teller Effect, Cambridge University Press, Cambridge, 2006, https://doi.org/10.1017/CB09780511524769.
- [19] I.B. Bersuker, Pseudo-Jahn-teller effect a two-state paradigm in formation, deformation, and transformation of molecular systems and solids, Chem. Rev. (2013) 113 1351–1390.
- [20] U. Öpik, M.H.L. Pryce, Studies of the jahn-teller effect. I. A survey of the static problem, Proc. R. Soc. London, A 238 (1215) (1997) 425–447, https://doi.org/ 10.1098/rspa.1957.0010.
- [21] L.E. Orgel, The stereochemistry of B subgroup metals. Part II. The inert pair, J. Chem. Soc. (1959) 3815–3819.
- [22] Maaskant, W. J. A., A combined jahn-teller and pseudo-jahn-teller effect illustrated by distortions of octahedra observed in yellow and red InCl. New J. Chem. 17(1–2), 97-105.
- [23] G.A. Gehring, K.A. Gehring, Co-operative Jahn-Teller effects, Rep. Prog. Phys. 38 (1975) 1–89.
- [24] B. Aurivillius, L. Sillén, Polymorphy of bismuth trioxide, Nature 155 (1945) 305–306, https://doi.org/10.1038/155305a0.
- [25] D.C. Craig, N.C. Stephenson, Structural studies of some body-centered cubic phases of mixed oxides involving Bi2O3: the structures of Bi25FeO40 and Bi38ZnO60, J. Solid State Chem. 15 (1) (1975) 1–8, https://doi.org/10.1016/0022-4596(75) 90264-9.
- [26] W. Kohn, L.J. Sham, Self-consistent equations including exchange and correlation effects, Phys. Rev. 140 (4) (1965) A1133–A1138, https://doi.org/10.1103/ PhysRev.140.A1133.
- [27] J.P. Perdew, K. Burke, M. Ernzerhof, Generalized Gradient Approximation Made Simple, 1996.
- [28] Blöchl, P. E. Projector augmented-wave method. Phys. Rev. B, 50(24), 17953-17979 doi:10.1103/PhysRevB.50.17953.
- [29] P. Giannozzi, et al., Quantum espresso: a modular and open-source software project for quantum simulations of materials, J. Phys. Condens. Matter 21 (2009).
- [30] P. Giannozzi, et al., Advanced capabilities for materials modelling with Quantum ESPRESSO, J. Phys. Condens. Matter 29 (2017).
- [31] H.J. Monkhorst, J.D. Pack, Special points for brillouin-zone integrations, Phys. Rev. B 13 (12) (1976) 5188–5192, https://doi.org/10.1103/PhysRevB.13.5188.

- [32] Murnaghan, F. D. The compressibility of media under extreme pressures. Proc. Natl. Acad. Sci. USA, 30(9), 244-247 doi:10.1073/pnas.30.9.244.
- [33] A.D. Becke, K.E. Edgecombe, A simple measure of electron localization in atomic and molecular systems, J. Chem. Phys. 92 (1990) 5397–5403, https://doi.org/ 10.1063/1.458517.
- [34] B. Silvi, A. Savin, Classification of chemical bonds based on topological analysis of electron localization functions, Nature 371 (1994) 683–686, https://doi.org/ 10.1038/371683a0.
- [35] A. Savin, H.-J. Flad, J. Flad, H. Preuss, H.G. von Schnering, On the bonding in carbosilanes, Angew. Chem., Int. Ed. Engl. 31 (1992) 185–187, https://doi.org/ 10.1002/anie.199201851.
- [36] R. Seshadri, N.A. Hill, Visualizing the role of Bi 6s "lone pairs" in the off-center distortion in ferromagnetic BiMnO3, Chem. Mater. 13 (9) (2001) 2892–2899.
- [37] V.L. Deringer, A.L. Tchougréeff, R. Dronskowski, Crystal orbital Hamilton population (COHP) analysis as projected from plane-wave basis sets, J. Phys. Chem. 115 (21) (2011) 5461–5466, https://doi.org/10.1021/jp202489s.
- [38] S. Maintz, V.L. Deringer, A.L. Tchougreeff, R. Dronskowski, J. Comput. Chem. 37 (2016) 1030–1035.
- [39] S. Maintz, V.L. Deringer, A.L. Tchougreeff, R. Dronskowski, J. Comput. Chem. 34 (2013) 2557–2567.
- [40] R. Nelson, C. Ertural, J. George, V.L. Deringer, G. Hautier, R. Dronskowski, LOBSTER: local orbital projections, atomic charges, and chemical-bonding analysis from projector-augmented-wave-based density-functional theory, J. Comput. Chem. 41 (21) (2020) 1931–1940, https://doi.org/10.1002/jcc.26353.
- [41] K.C. Pitike, W.D. Parker, L. Louis, S.M. Nakhmanson, First-principles studies of lone-pair-induced distortions in epitaxial phases of perovskite SnTiO3 and PbTiO3, Phys. Rev. B Condens. Matter 91 (2015).
- [42] H.-.-H. Schmidtke, I.B. Bersuker, V.Z. Polinger, Vibronic Interactions in Molecules and Crystals, 49 aus, Springer Series in Chemical Physics. Springer-Verlag Berlin, Heidelberg, New York, London, Paris, Tokyo, 1990, pp. 896–897, https://doi.org/10.1002/bbpc.19900940819, 1989. 422 Seiten, Preis: DM 178,—.. Berichte der Bunsengesellschaft für physikalische Chemie, 94.
- [43] N.I. Medvedeva, V.P. Zhukov, D.L. Novikov, V.A. Gubanov, Electronic structure and chemical bonding of δ-Bi2O3, J. Struct. Chem. 37 (1996) 41–50.
- [44] D.B. P, R.A.C. C, D. J, D.M. A, The structural properties of the oxygen conducting δ phase of Bi2O3, J. Phys. C Solid State Phys. 16 (17) (1983) L561, https://doi.org/10.1088/0022-3719/16/17/003.
- [45] B. Aurivillius, G. Malmros, Kungl. Tekniska Högskolans Handlingar 291 (1972) 545—562.
- [46] S. Hull, S.T. Norberg, M.G. Tucker, S.G. Eriksson, C.E. Mohn, S. Stolen, Neutron total scattering study of the δ and β phases of Bi₂O₃, Dalton Trans. (2009) 8737–8745.
- 47] S.K. Blower, C. Greaves, The structure of β-Bi₂O₃ from powder neutron diffraction data, Acta Crystallogr. C 44 (1988) 587–589.
- [48] N. Jiang, E.D. Wachsman, Structural stability and conductivity of phase-stabilized cubic bismuth oxides, J. Am. Ceram. Soc. 82 (1999) 3057–3064, https://doi.org/ 10.1111/j.1151-2916.1999.tb02202.x.
- [49] A. Walsh, et al., Electronic structure of the α and δ phases of Bi₂O₃: a combined ab initio and x-ray spectroscopy study, Phys. Rev. B Condens. Matter 73 (2006).
 [50] D. Pérez-Mezcua, I. Bretos, R. Jiménez, et al., Photochemical solution processing of
- [50] D. Pérez-Mezcua, I. Bretos, R. Jiménez, et al., Photochemical solution processing o films of metastable phases for flexible devices: the β-Bi₂O₃ polymorph, Sci. Rep. (2016), 39561.
- [51] J. Wang, et al., Precursor-induced fabrication of beta-Bi2O3 microspheres and their performance as visible-light-driven photocatalysts, J. Mater. Chem. A. 1 (2013) 9069–9074
- [52] L.G. Sillen, Ark. Kemi. Mineral. Geol, 1937, pp. 1–15, 12A.
- [53] W.P. Doyle, J. Phys. Chem. Solid. 4 (1958) 144.
- [54] A. Laarif, F. Theobald, The lone pair concept and the conductivity of bismuth oxides Bi₂O₃, Solid State Ionics 21 (1986).
- [55] Abdul Hameed, Tiziano Montini, Valentina Gombac, Paolo Fornasiero, Surface phases and photocatalytic activity correlation of Bi₂O₃/Bi₂O_{4-x} nanocomposite, J. Am. Chem. Soc. 130 (30) (2008) 9658–9659.
- [56] M. Vila, C. Díaz-Guerra, J. Piqueras, Luminescence and Raman study of α-Bi₂O₃ceramics, Mater. Chem. Phys. 133 (1) (2012).
- [57] B. Tsukerblat, The jahn-teller effect. By isaac B. Bersuker, Angew. Chem. Int. Ed. 45 (2006) 8089–8090, https://doi.org/10.1002/anie.200685413.
- [58] A.M. Glazer, J. Appl. Crystallogr. 42 (2009) 1194-1196.